Chapter 5. Modeling the Transverse Compression of Wood-Based Composites

Summary

The vertical density profile has been identified as one of the most important characteristics that determines panel strength and physical properties. The vertical density profile formation is the result of many interacting process variables. During the compression process the mat is in an unsteady state resulting in continuously changing internal conditions (temperature and moisture content) as the pressing operation proceeds. Therefore, the vertical density profile is formed not only during the consolidation, but well after the panel has reached the target thickness. No satisfactory attempt was made to fully understand the process. A model can help to address this need and infer the relationship between processing parameters and density profile formation. A comprehensive analysis of the consolidation process during hot-pressing must examine the viscoelastic behavior of the flakes in transverse compression. The transverse compression behavior is highly nonlinear due to the cellular structure of the flake mat. Additionally, the mechanical properties of the flakes show typical viscoelastic behavior, with time, temperature, and moisture dependence. A nonlinear viscoelastic compression model was developed which separates the geometric nonlinear response of the cellular structure of the flakes from the linear viscoelastic response of the cell wall polymers. The behavior of the cellular structure is modeled with the modified Hooke's Law, which includes an additional nonlinearizing term. The viscoelastic properties of the flakes are described by the time-temperature-moisture equivalence principle of polymers. Two separate models were developed based on the integration of the above theories. The first model is based on the representation of material behavior with a series of Maxwell ladders. An alternative simplified model was developed due to excessive solution time. The nonlinear viscoelastic compression model can simulate the formation of the average vertical density profile under a wide variety of pressing conditions.

5.1 Introduction

During the hot-pressing cycle, heat and pressure is applied simultaneously to consolidate the loosely formed flake mat to the final panel. The heat is transported from the hot platens vertically to the center of the mat by conduction and convection. The water content of the flakes close to the hot platens is vaporized, and the water vapor migrates towards the cooler center vertically, and to the edges of the mat horizontally. This simultaneous heat and mass transfer results in transient temperature, gas pressure, and moisture content gradients in the mat, as was demonstrated in the previous two chapters. Additionally, a high compaction pressure (4-13 MPa) is imposed on the mat structure during the press closing time to consolidate the mat to the target thickness. Because of the uneven horizontal thickness distribution of the mat, the localized pressure can be above the compaction pressure. Although the press position is kept at the target thickness after the consolidation, the ram pressure continuously declines during the rest of the press period due to stress relaxation in the mat. The transient temperature and moisture content gradient result in non-uniform, continuously changing compression properties of the wood components. The viscoelastic (time, temperature, moisture dependent) properties of the adhesive also continuously change during the hot-compression, while the adhesive polymerizes into a three dimensional network. The contribution of the adhesive viscoelastic behavior to the behavior of the wood-adhesive system is complex, and not clearly understood. Additionally, the most deformation occurs within the wood part of the composite material, and therefore, the wood dominates the viscoelastic behavior of the whole system. Consequently, the effect of the adhesive on the viscoelastic properties of the composite is not addressed in this study, and the main focus was given to the description of the wood material response during the compression. As the compaction pressure is coupled with the changing viscoelastic properties of the wood, a density gradient develops in the processed panel. The venting period is initiated in the press schedule after the resin is adequately cured in the center of the mat. The press slowly opens, and the compaction pressure is relieved. The panel gains thickness (spring back) as the residual stresses are released, forming the final density profile in the panel. The vertical density profile is one of the main characteristic which determines the mechanical properties of the panel. Therefore, the establishment of the relationship between pressing parameters and the final density profile is crucial to optimize final panel properties.

5.2 Background

In spite of the known effect of pressing parameters on the vertical density profile of the final panel, only a few attempts were made to model the formation of the density profile. The limited number of models concentrate on different aspects of the hot-compression process, and most of them make oversimplifications about the involved mechanisms.

Several researchers modeled the nonlinear stress-strain behavior of the cold compression process based on transverse compression theories of cellular materials (Wolcott 1989, Dai and Steiner 1993, Dai et al. 1997, Lenth and Kamke 1996a, b, Lang and Wolcott 1995, 1996). Although these models are capable predicting the rapid increase of compression stresses during the consolidation process with varying degrees of accuracy, they miss an important element of the pressing operation, that the compression behavior of the flakes is changing with temperature and moisture content. Consequently, these models are not applicable to hot-compression simulation and unable to predict the vertical density profile formation through the thickness of the mat. Therefore, it has been recognized that a computer simulation model is needed to investigate the complex effect of heat and mass transfer on the final vertical density profile.

Harless et al. (1987) were among the first to attempt to model the development of the density profile in particleboard. Their model included the heat conduction, gas transport, water phase change, and layer compaction mechanisms. The model is essentially a one-dimensional model and it terminates as the target thickness of the board is reached, excluding the influence of the changing internal environment on the differential relaxation of the flakes in the remainder of the press cycle.

Suo and Bowyer (1994) simulated the formation of the density profile of particleboard. They subdivided the mat through the thickness to thin uniform density layers. The compression properties of these layers were determined as a function of the changing temperature and moisture content conditions. The strain of each layer was calculated during the consolidation, and the changing thickness of the layers formed the density profile.

A modular finite-element computer simulation of the hot-compression of wood-based composites was developed by Hubert and Dai (1997). The model is one-dimensional and only final density profile predictions were reported, with no reference to the time dependent formation of the profile.

All of the previous models consider the dynamic conditions during the consolidation process, but ignore the density profile formation after the compaction period. However, Wolcott and Kamke (1990, 1994) provided ample evidence that the density profile is formed during the entire pressing cycle.

Additionally, several experimental studies with a γ-ray in-situ density measurement system also reinforced that the profile is formed after the press closing (Winistorfer et al. 2000, Wang and Winistorfer 2000a, b).

The deficiencies of the previous models were recognized by Humphrey and Thoemen (2000) and the most comprehensive continuous hot-compression model for wood-based composites, which can predict the density profile formation during the entire pressing operation, was developed. The model includes heat and mass transfer, adhesion kinetics, and the hygro-thermo-compressibility of the flake mat.

The following chapter summarizes the third stage of the research, which was the development of a transverse compression model for the consolidation of wood-based composites. The time, temperature, and moisture dependence of wood under transverse compression, together with the nonlinear stress development, were incorporated in the model.

5.3 Model Development

5.3.1 Nonlinear Transverse Compression Behavior of the Wood Flakes

Cellular materials generally show a characteristic non-linear behavior during transverse compression, resulting from the collapse of the cellular structure. Figure 5.1 shows a typical non-linear stress-strain curve of a cellular solid in transverse compression.

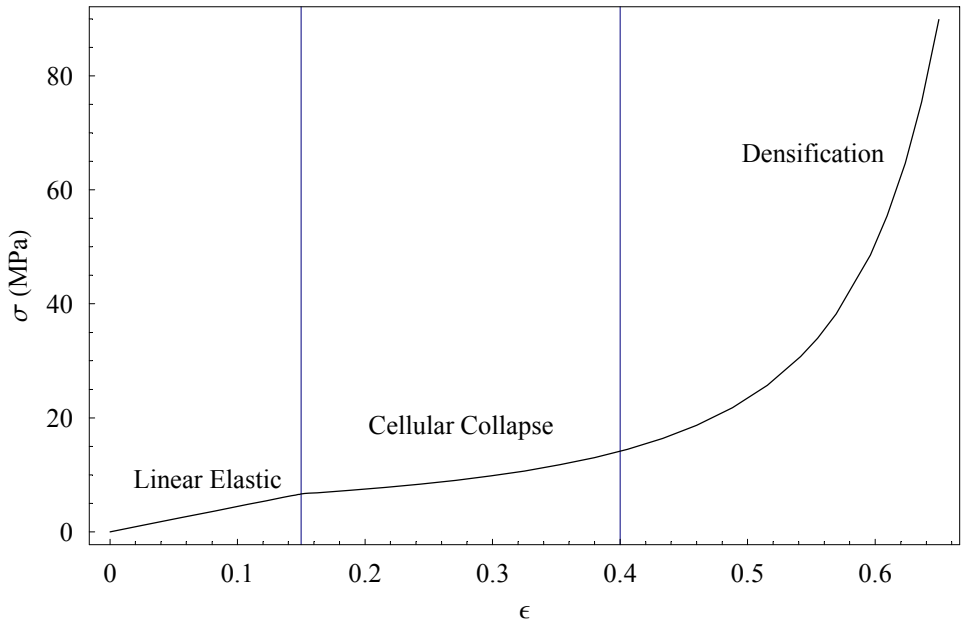

Figure 5.1. Characteristic stress-strain diagram for cellular materials.

Three characteristic regions can be observed in both man-made and natural cellular materials: linear elastic, cellular collapse, and densification. The material at the beginning of compression deforms in a linear elastic manner. At the onset of cellular collapse, the cell wall material yields, and due to the cumulative collapse of the cell walls, the material continues to deform at a nearly constant stress level. Cellular collapse occurs either by elastic buckling, plastic yielding or brittle crushing, depending on the type of the cell wall material. Different fracture mechanisms result in different stress-strain behavior. However, Wolcott (1989) demonstrated that elastic buckling is a viable assumption as the form of collapse of the wall of wood cells. At the end of the collapse region the cell wall structure starts to consolidate. At this point most of the cells are collapsed, and opposing cell walls are in good contact. The characteristic of the densification region is the rapid stress increase as the compression continues. These regions are present in all types of cellular structures, but the initiation and the length of the regions are a function of the cell geometry. The cell geometry is characterized by the relative density (ρ_r), which is defined as the ratio of the density of the cellular material to the density of the cell wall material.

The Young's modulus of the cellular material is related to the Young's modulus of the cell wall (E_{cw}) and the cellular geometry represented by the relative density (ρ_r), as follows (Gibson and Ashby 1997):

$$E = E_{cw}\,\rho_r^3 \tag{5.1}$$

where

E = Young's modulus of the cellular material,
E_{cw} = Young's modulus of the cell wall,
ρ_r = relative density.

This equation states that the Young's modulus (E) of any wood species could be derived as the product of the constant cell wall modulus (variation of the cell wall modulus is negligible for different species) and the relative density (related to the specific gravity) of the species. Consequently, the modulus of the wood species is only a function of the cellular structure, as represented by the relative density. This has utmost importance; once it is possible to determine the temperature and moisture dependence of the cell wall modulus, the Young's modulus of any species at any temperature and moisture content, could be determined by the above equation without additional testing. The mechanical testing of separated cell wall material has not yet been solved. Therefore, the time, temperature, moisture dependence of the Young's modulus (relaxation modulus) of each species has to be determined with separate mechanical testing. The experimental determination of the relaxation modulus of yellow poplar (*Liriodendron tulipifera*) will be discussed in the following section (see Deriving the Stress Relaxation Curve).

The characteristic shape of the stress-strain curve can be described by a non-linear multiplier ($\psi(\epsilon)$) in the modified Hooke's Law, called the nonlinear strain function, as follows:

$$\sigma = E\,\epsilon\,\psi(\epsilon) \tag{5.2}$$

where

σ = stress,
E = Young's Moduls,
ϵ = strain,
$\psi(\epsilon)$ = nonlinear strain function.

The influence of the geometry of the cellular structure on the consolidation behavior of the material is accounted for by the non-linear strain function. It can be determined experimentally (Meinecke and Clark 1973) or from the characteristic plastic strain observed in a stress-strain diagram (Rusch 1969).

However, Maiti et al. (1984) derived a relationship between the nonlinear strain function and the applied strain based on the yield strain of the cell wall material, as follows:

$$\psi(\epsilon) = 1; \qquad \epsilon \le \epsilon_y$$
$$\psi(\epsilon) = \frac{\epsilon_y}{\epsilon}\left(\frac{1-\rho_r^{1/3}}{1-\rho_r(\epsilon)^{1/3}}\right)^3; \qquad \epsilon > \epsilon_y \tag{5.3}$$

where

ϵ_y = yield strain of the cell wall,
ϵ = applied strain,
ρ_r = relative density,
$\rho_r(\epsilon)$ = relative density function.

The nonlinear strain function $\psi(\epsilon)$ is a nonlinear multiplier of the stress calculated by assuming linear behavior. It depends on the strain and relative density. Therefore, it essentially monitors the cellular collapse in the material as a function of the cellular structure. Figure 5.2 depicts the non-linear strain function at different relative densities.

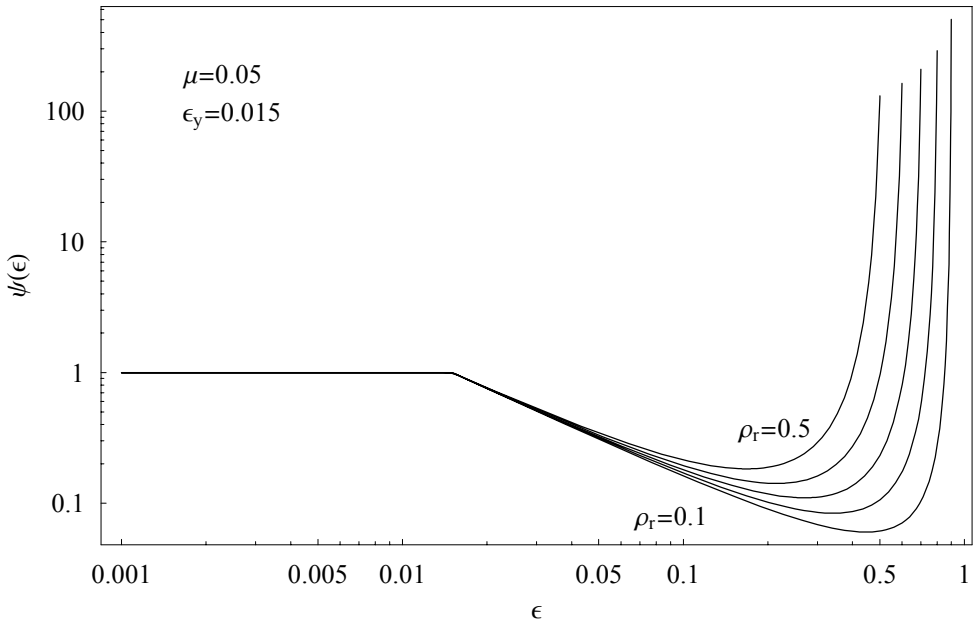

Figure 5.2. The nonlinear strain function $\psi(\epsilon)$ as a function of relative density ρ_r.

This nonlinearizing function separates the linear elastic region from the collapse, and densification regions. Therefore, it is capable of describing the stress development during the full range of the transverse compression of cellular materials. The yield strain of the cell wall of wood was determined by Wolcott (1989) as 0.015. The nonlinear strain function has a value of unity when the strain is below the yield strain of the cell wall. In this case the modified Hook's

Law returns to the ordinary Hook's Law describing the linear elastic behavior of the cell wall under low levels of strain. During the cellular collapse region the non-linear strain function decreases until it reaches a minimum value at the onset of densification of the cell wall material. During the densification region, the nonlinear strain function increases and approaches infinity with increasing strain.

The relative density of the material increases during the transverse compression of the cellular structure. The relative density function ($\rho_r(\epsilon)$) takes into consideration this dilatation effect. In the case of elastomeric foams, no significant lateral expansion occurs, even within the nonlinear region of the stress-strain curve. Therefore, the following equation adequately monitors the relative density changes:

$$\rho_r(\epsilon) = \rho_r(1 - (\epsilon - \epsilon_y))^{-1} \tag{5.4}$$

However, in the case of wood, a lateral expansion can be observed in the radial or tangential direction during transverse compression, called the "barrelling effect" (Kasal 1989). When the loaded surfaces are restrained, the shape of the lateral expansion can be described by a parabola (Figure 5.3).

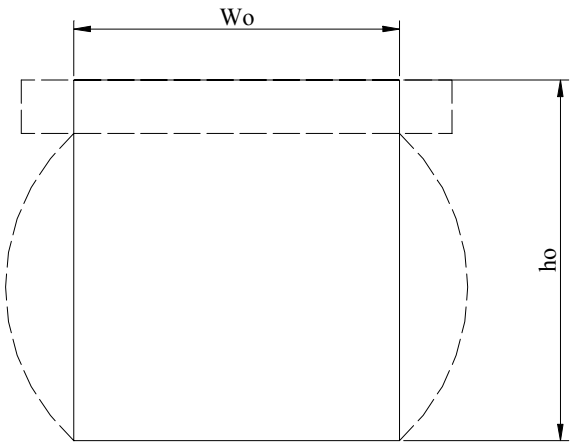

Figure 5.3. The "barrelling effect" of wood under transverse compression. W_0 and h_0 are the initial width and height of the specimen.

Therefore the previous equation has to be modified as follows (Kasal 1989):

$$\rho_r(\epsilon) = \rho_r\left(1 - (\epsilon - \epsilon_y) + \frac{2}{3}\mu(\epsilon - \epsilon_y) - \mu(\epsilon - \epsilon_y)^2\right)^{-1}, \tag{5.5}$$

where

μ = expansion ratio.

A new term, called expansion ratio (μ) is defined, which is the ratio of lateral strain to compressive strain in the nonlinear stress-strain region. It was found experimentally that the expansion ratio is a function of specimen height (Wolcott 1989). The expansion ratio is larger for taller specimens, because the frictional restrictive effect of the loading surfaces is not as pronounced. Figure 5.4 depicts the non-linear strain function as a function of the expansion ratio.

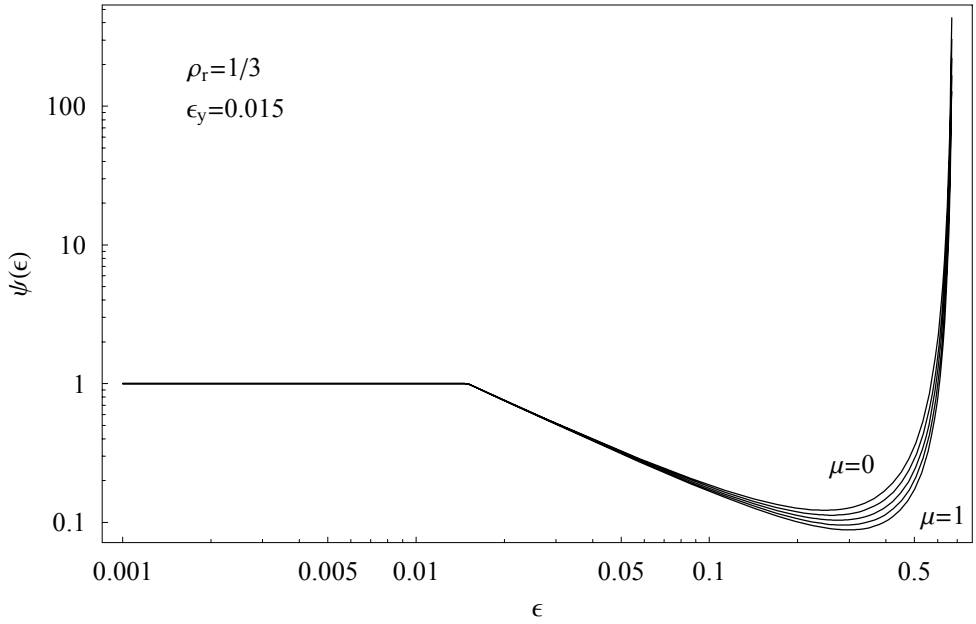

Figure 5.4. The nonlinear strain function $\psi(\epsilon)$ as a function of expansion ratio μ.

The applicability of the cellular material compression theories to describe the nonlinearity of the transverse compression of solid wood was demonstrated by several researchers (Wolcott 1989, Kasal 1989, Esterling et al.1982, Lenth 1994, Lenth and Kamke 1996a, 1996b). This theory will characterize the nonlinear stress development during the consolidation of the flake mat.

5.3.2 Viscoelastic Behavior of the Wood Flakes

5.3.2.1 Plasticization of the Wood Flakes

The rapidly changing internal environment affects the mechanical properties of the flakes during the hot-pressing. In spite of the large variety of wood species, all of them are formed from the same polymers, namely cellulose, lignin, and hemicelluloses. Considering the wood flakes as a polymer system opens up the possibility to unify the effect of time, temperature, and moisture on the mechanical properties based on the viscoelastic theory of polymers.

Viscoelastic theory states that amorphous polymers can show a range of mechanical properties from viscous fluids to elastic solids depending on the time scale, the ambient temperature, and the diluent concentration (Figure 5.5). The polymer changes from a "glassy phase", which is characterized by high modulus, to a "rubbery phase" where the modulus is three orders of magnitude lower as time, temperature, and moisture content increase. Between these two extreme conditions the polymer is at a transition "leathery phase". In this region a small change in time, temperature, and moisture content can result in a large change in polymer properties.

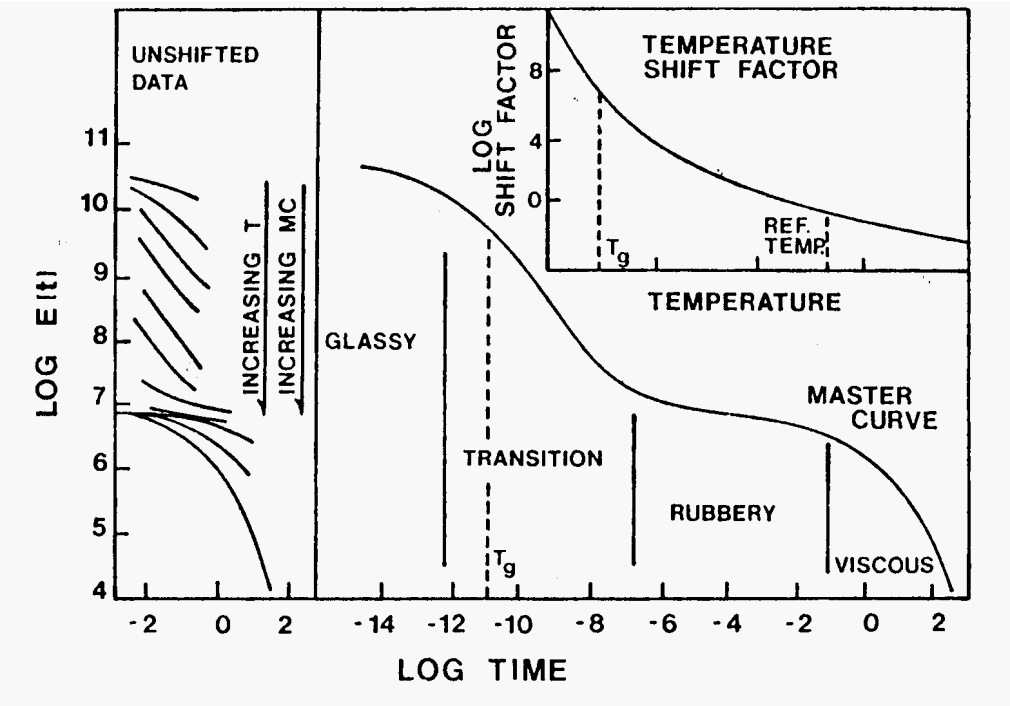

Figure 5.5. Typical change of the relaxation modulus ($E(t)$) of an amorphous polymer with time and temperature.

The material property which describes the phase change in the polymer related to temperature increase is the glass transition temperature (T_g). Below the glass transition temperature the molecular motion is limited and the mechanical properties are only slightly affected by temperature. The polymer is in the glassy state. As the glass transition temperature is approached the molecules have increasing mobility and the mechanical properties, especially the stiffness of the material, are decreased substantially, and the polymer is at the transition phase. Further increase in temperature causes the polymer to enter the rubbery phase. The magnitude of the glass transition temperature has been attributed to the free volume of the polymer (Ferry 1980). The free volume is defined as the difference between the occupied volume and the specific volume of the polymer (Billmeyer 1984). The slope of the specific volume versus temperature curve increases at the glass transition temperature. The free volume is relatively constant in the glassy phase, and increases linearly with the temperature above T_g. The increasing free volume above T_g can be related to the increasing molecular mobility.

The free volume is also affected by the diluent concentration (moisture content). Free volume increases together with the diluent concentration. Consequently, the T_g of the polymer decreases. Kwei (1984) investigated the effect of diluent concentration on the T_g of diluent-polymer mixtures. He derived a universally applicable model. This model accounts for, not only the effect of free volume changes on the glass transition temperature, but also the effect of secondary interactions between the polymer molecules and the diluent.

The equation proposed by Kwei (1984) is:

$$T_g = \frac{T_{g1}\, W_1 + k\, T_{g2}\, W_2}{W_1 + k\, W_2} + q\, W_1\, W_2 \qquad (5.6)$$

where

T_g = glass transition temperature of the polymer – diluent mixture,
W = weight fraction,
k = adjustable parameter for free volume effects (lignin : 10, hemicellulose : 13),
q = adjustable parameter for secondary interactions (lignin : 585, hemicellulose : 355),
1, 2 = denote polymer and diluent respectively,
T_{g1} = 200 °C for lignin and hemicellulose,
$T_{g2} = -137$ ° for water.

The first term of the equation describes the free volume dependence of T_g, the second term is proportional to the number of secondary interactions between the polymer and the diluent. Water is mainly attached to the free -OH groups of the lignin and hemicelluloses and acts as a diluent. Increasing moisture content decreases the T_g of the lignin and hemicelluloses in wood (Salmen 1984, Kelley et al. 1987). Kelley et al. (1987) proved the applicability of the

Kwei equation to describe the moisture content dependence of the T_g of the moisture-wood system. Wolcott and Kamke (1990, 1994) applied the equation to predict the T_g as a function of moisture content of yellow-poplar flakes. Only the lignin component was considered during the calculation of the T_g of wood. Figure 5.6 shows the moisture dependence of the T_g of hemicellulose and lignin based on the Kwei equation.

Based on the previous theories, when wood is in a high temperature environment in the presence of water, the phenomena of plasticization occurs. The modulus of the material decreases several orders of magnitude. Plasticization is desirable during wood-based composite manufacture, because it reduces the fracture of the wood particles under the applied compression stresses and ensures more intimate flake contact, and therefore, better adhesive bonds. The glass transition temperature (T_g) will determine whether the wood constituent polymers (cellulose, lignin, hemicelluloses) are in the glassy or rubbery phase. Several investigations focused on the determination of the glass transition temperature of the separated chemical constituents of wood (Salmen and Back 1977, Salmen 1984, Salmen et al. 1985). Although the highly crystalline cellulose includes amorphous regions, the contribution of these regions to the viscoelastic properties of wood is negligible (Salmen et al. 1985). Hemicelluloses are branched polymers and their T_g is low, below room temperature. It can be assumed that hemicelluloses are in the rubbery phase throughout the temperature and moisture range during hot-pressing (Back and Salmen 1982, Funokashi et al. 1979). Therefore it can be concluded that the glass transition and plasticization of wood are controlled by the amorphous lignin.

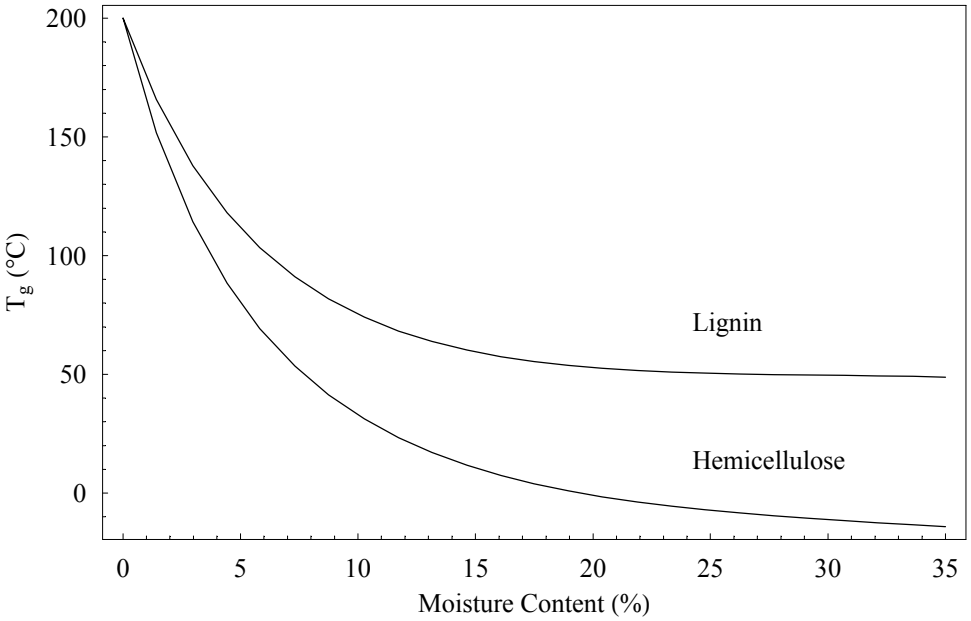

Figure 5.6. Diluent dependence of T_g of lignin and hemicellulose as described by the Kwei model.

The plasticization phenomena can be represented with the viscoelastic polymer properties, such as the creep compliance (D(t)) and relaxation modulus (E(t)). The viscoelastic properties are affected by time, temperature, and moisture. The relationship is described by the time-temperature-moisture equivalence principle (Williams et al. 1955). The basis of the principle is that temperature and moisture merely accelerate the time-dependent response of the material. The time-temperature-moisture content superposition is an accelerated testing technique based on the equivalence principle. The time-dependent material properties are determined at different moisture and temperature levels and shifted horizontally along the log-time axis through a time multiplier (shift factor), until a smooth curve is created. The so called "master curve" describes the time dependence of the investigated property at a reference temperature and moisture content. The property is calculated at other temperature and moisture levels with the reduced time principle, and shift factors.

The observation of the time-temperature-moisture superposition was originally empirical. However, a theoretical basis has been developed based on free volume theory (Ferry 1980). The temperature shift factors can be calculated based on the free volume concept. When the glass transition temperature of the polymer is chosen as the reference temperature, the temperature shift factor can be determined below T_g by an Arrhenius-type equation:

$$\log a(T) = \frac{\Delta \mathrm{E}}{2.303 \cdot R} - \left(\frac{1}{T} - \frac{1}{T_g} \right), \tag{5.7}$$

where

$a(T) =$ temperature shift factor,
$\Delta \mathrm{E} =$ activation energy,
$R =$ universal gas constant,
$T_g =$ glass transition temperature,
$T =$ temperature.

Above T_g the Williams-Landell-Ferry (WLF) equation gives the temperature shift factor:

$$\log a(T) = \frac{-C_1 \cdot (T - T_g)}{C_2 + T - T_g}, \tag{5.8}$$

where

$C_1 =$ universal WLF constant,
$C_2 =$ universal WLF constant.

The constants (C_1, C_2) of the WLF equation were determined experimentally for several amorphous polymers (Alkonis 1983, Rosen 1993). It was found that different polymers have very similar WLF constants. Therefore, "universal" constants were established for cases when the experimental determination is not feasible ($C_1 = 17.44$, $C_2 = 52.1$). A drawback of the theoretical method is that the inclusion of the moisture dependence of the shift factor is complex. Therefore, the temperature and moisture shift factor, a(T, M), used in this study was determined by Wolcott (1989) experimentally.

5.3.2.2 Mathematical Representation of Viscoelastic Behavior

According to the linear viscoelastic theory, the time-dependent response of a viscoelastic material, for an arbitrary loading history, can be expressed either in an integral or a differential form, if a single creep or relaxation curve for a prolonged time period is available (e.g. experimentally collected).

The integral form of the mathematical representation of linear viscoelasticity is based on the superposition principle. It states that the effect of a complex loading history can be equated to the sum of independent contributions of smaller load steps. Therefore, the time dependent response to the sum of independent load steps is expressed by a convolution integral, called the Boltzmann Superposition Integral. The Boltzmann Integral takes the following form to represent the time dependent strain ϵ(t) during the creep phenomenon

$$\epsilon(t) = D(t)\,\sigma(0) + \int_0^t D(t-\xi)\,\frac{d\sigma}{d\xi}\,(\xi)\;d\xi\,. \tag{5.9}$$

The time dependent stress relaxation σ(t) can be described as

$$\sigma(t) = E(t)\,\epsilon(0) + \int_0^t E(t-\xi)\,\frac{d\epsilon}{d\xi}\,(\xi)\;d\xi\,. \tag{5.10}$$

The use of the integral requires that either the creep compliance (D(t)), or the stress relaxation modulus (E(t)) be expressed analytically (e.g. a function fitted to measured data). Additionally, the Boltzmann Integral is restricted to linear materials. Direct derivation of the integrals to describe the behavior of nonlinear materials is not reported. The extension of the Boltzmann Integral for nonlinear materials was proposed by Meinecke and Clarck (1973). If the material is not strained initially, the time dependent stress response of a nonlinear material is described by the following equation:

$$\sigma(t) = \int_0^t E(t-\xi)\,\frac{d\epsilon}{d\xi}\,(\xi)\;\psi(\epsilon(\xi))\,d\xi\,, \tag{5.11}$$

where

$\psi(\epsilon(\xi))$ = nonlinear strain function.

The solution of this integral depends on the complexity of the $\psi(\epsilon(\xi))$ term. It was pointed out by Meinecke and Clarck (1973) that the simplification of the integral still reaches sufficient accuracy:

$$\sigma(t) = \psi(\epsilon(t)) \int_0^t E(t-\xi) \frac{\mathrm{d}\epsilon}{\mathrm{d}\xi}(\xi)\, d\xi \,. \tag{5.12}$$

This equation indicates that once the solution of the integral of linear viscoelastic behavior is known, the result only has to be multiplied by the nonlinear strain function $\psi(\epsilon(t))$.

The differential form of the mathematical representation of linear viscoelasticity is based on the governing differential equations of mechanical analogies, such as combined spring and dashpot elements. The analogies are phenomenological, therefore, they describe the observed phenomena adequately, but there is no physical insight into the problem. A Kelvin element (a spring and a dashpot in parallel) represents the creep behavior, and a Maxwell element (a spring and a dashpot in series) represents the stress relaxation. The governing differential equations for the Kelvin and Maxwell element are respectively:

$$\frac{\partial \epsilon}{\partial t} = \frac{D}{\tau}\sigma - \frac{1}{\tau}\epsilon, \tag{5.13}$$

$$\frac{\partial \sigma}{\partial t} = E\frac{\partial \epsilon}{\partial t} - \frac{1}{\tau}\sigma, \tag{5.14}$$

where

τ = retardation or relaxation time = $\frac{\eta}{E}$,
E = modulus of the spring,
η = viscosity of the dashpot,
D = compliance of the spring = $\frac{1}{E}$.

The solution of the previous differential equations provide the time dependent response of the Kelvin and Maxwell element for a step load as follows:

$$\epsilon(t) = \sigma(0)\, D\left(1 - e^{\frac{-t}{\tau}}\right), \tag{5.15}$$

$$\sigma(t) = \epsilon(0)\, E\, e^{\frac{-t}{\tau}}. \tag{5.16}$$

In order to produce a more realistic time dependent material response, Kelvin elements are combined in series and Maxwell elements in parallel. These are referred to as a Kelvin chain, and Maxwell ladder (Figure 5.7).

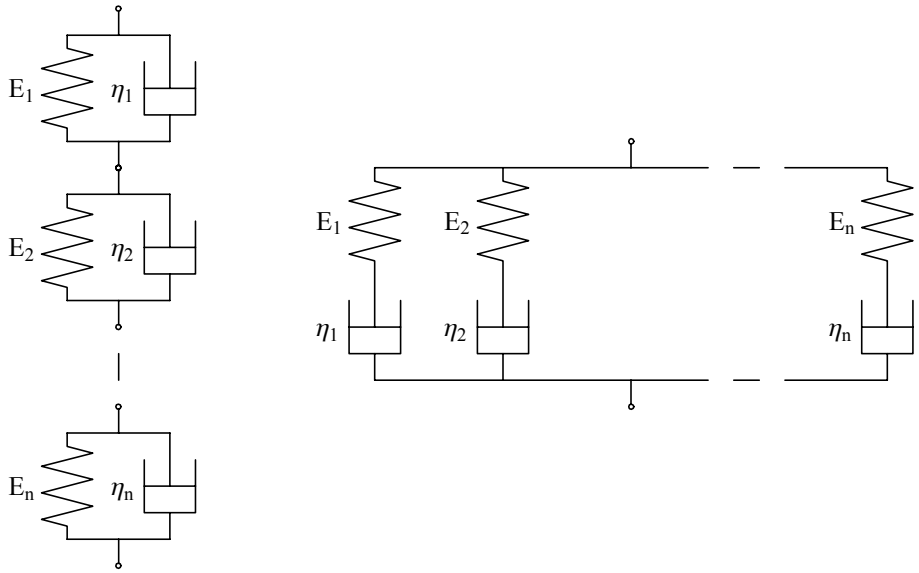

Figure 5.7. Linear viscoelastic models: Kelvin chain and Maxwell ladder.

Ten to fifteen connected elements are adequate to reach good agreement between the experimental and the predicted creep and stress relaxation curves.

The time dependent creep of a Kelvin chain for a step load is given by

$$\epsilon(t) = \sigma(0) \sum_{i=1}^{n} \frac{1}{E_i} \left(1 - e^{\frac{-t}{\tau_i}}\right), \tag{5.17}$$

while the time dependent stress relaxation for a step load is given by

$$\sigma(t) = \epsilon(0) \sum_{i=1}^{n} E_i \; e^{\frac{-t}{\tau_i}} \; . \tag{5.18}$$

For more complex loading conditions than a step load, the partial differential equations (E.q. 5.13, E.q. 5.14) have to be solved numerically.

5.3.2.3 Deriving the Stress Relaxation Curve

In order to calculate the time-dependent response of the flakes to a loading history, either with the integral or the differential form, the creep or relaxation response of the material for a prolonged time period is necessary. However, the prolonged testing of the material is not feasible. Therefore, the time-temperature-moisture superposition technique was used by Wolcott (1989) to experimentally determine the relaxation curves for a long time period. Wolcott measured the relaxation modulus (E(t)) of yellow-poplar (*Liriodendron tulipifera*) specimens in tension at six moisture content levels (3, 6, 8, 10, 12, 16 %) in the temperature range from 39-99 °C at 3 °C intervals. The separate curves measured at different temperatures, but at a common moisture content, were shifted on the log-time axis to a reference temperature of 60 °C. The individual temperature master curves were shifted again to a reference moisture content of 3 % to construct an overall master curve (Figure 5.8).

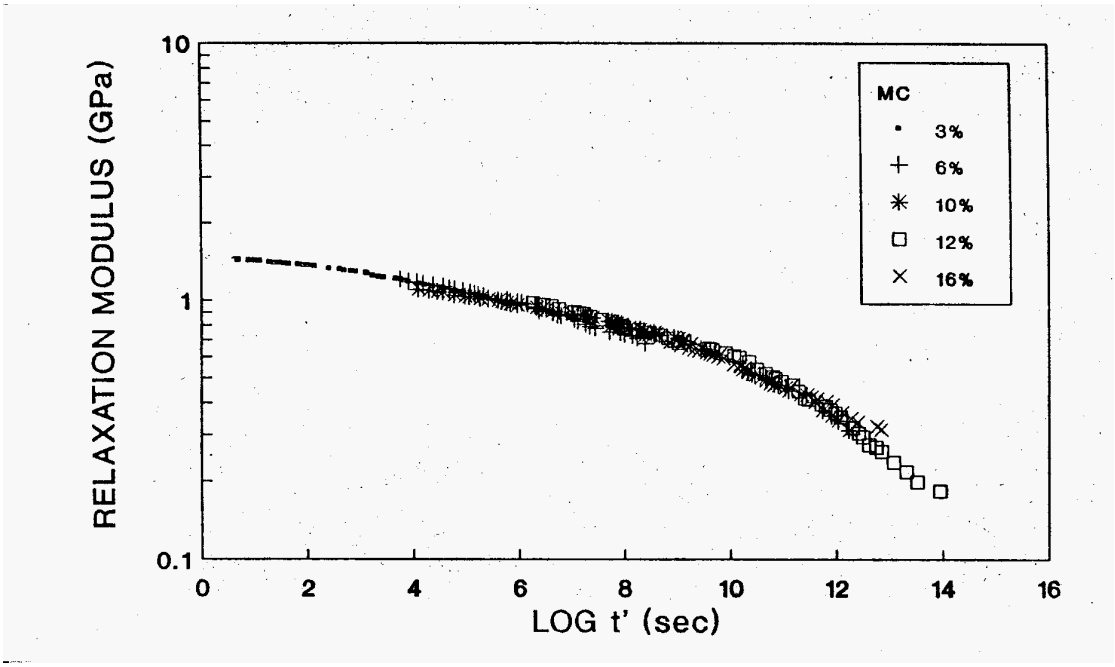

Figure 5.8. Relaxation modulus E(t') master curve plotted against reduced time (t'=t/a(T,M)). The master curve is shifted to a reference temperature of 60 °C and a moisture content of 3%. (Wolcott 1989)

The temperature shift factors were found to be linear functions of temperature at each moisture content. The parameters of the fitted linear equations are listed in Table 5.1. The moisture content shift factors are repeated here in Table 5.2.

Table 5.1. Parameters for the regression equations describing the temperature shift factor, log a(T) as a function of temperature for different moisture contents. The form of the equations are: $\log a(T) = Y_0 - b\,T$

Moisture Content (%)	Temperature (°C)	Y_0	b
3	57 – 72	6.125	0.1024
3	72 – 99	1.647	0.0413
6	39 – 99	2.763	0.0432
8	39 – 99	5.413	0.0832
10	39 – 99	5.887	0.0933
12	39 – 90	6.547	0.1128
16	39 – 75	5.770	0.0937

Table 5.2. Moisture shift factor, log a(M).

Moisture Content (%)	log a (M)
3	0
6	−4
8	−4.8
10	−5.8
12	−7
16	−9.2

The measured temperature and moisture shift factors were combined, and a second order equation was fit to the surface, as proposed by Maksimov et al. (1971, 1974, 1975, 1976):

$$\log a(T, M) = \alpha + \beta_1 \cdot T + \beta_2 \cdot T^2 + \beta_3 \cdot M + \beta_4 \cdot M^2 \qquad (5.19)$$

where

$a(T, M)$ = temperature and moisture shift factor,
T = temperature,
M = moisture,
α = 8.9361,
$\beta_1 = 1.027\,x\,10^{-1}$,
$\beta_2 = 1.361\,x\,10^{-4}$,
$\beta_3 = 1.1908$,
$\beta_4 = 2.598\,x\,10^{-2}$.

The "master curve" created by the time-temperature-moisture superposition allows the prediction of the stress relaxation modulus (E(t)) of the material within 16 decades of time at the reference 60 °C temperature and 3% moisture content (Figure 5.8). Furthermore, with the experimentally derived temperature and moisture shift factors (log a(T,M) Figure 5.9), the master curve can be shifted to different temperature and moisture levels with the reduced variable principle, as will be discussed in the following section. The shifted master curve can predict the viscoelastic properties of the flakes at varying internal mat conditions.The fitted temperature and moisture shift factor surface is depicted in Figure 5.9.

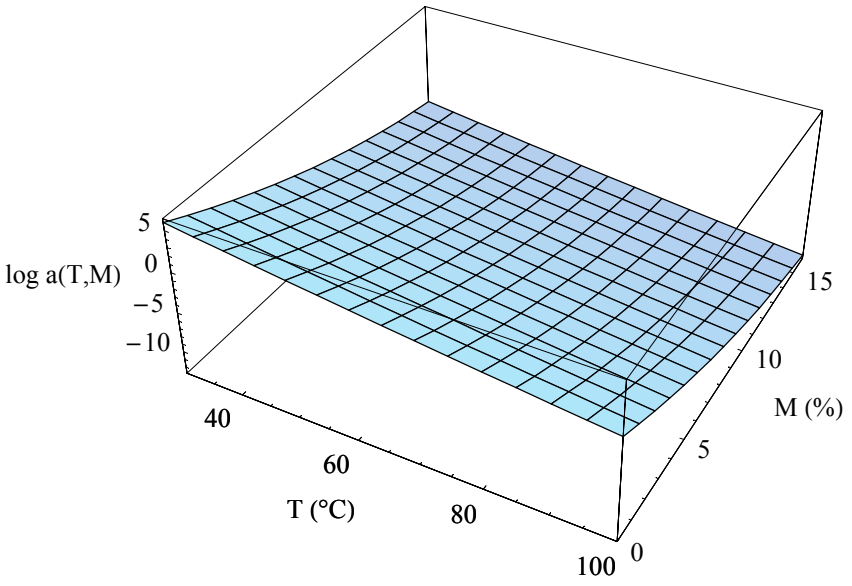

Figure 5.9. The temperature and moisture content shift factor (log a(T,M)). The second order surface was fit to data derived by Wolcott (1989).

The measured time-dependent viscoelastic properties can be represented mathematically. A convenient method to express E(t) and D(t) is with mechanical analogies. Creep is represented by a Kelvin chain, and relaxation by a Maxwell ladder. Therefore, the creep compliance and the relaxation modulus can be described with a finite exponential series form as follows:

$$D(t) = \sum_{i=1}^{n} \frac{1}{E_i} \left(1 - e^{-\frac{t}{\tau_i}}\right), \tag{5.20}$$

$$E(t) = \sum_{i=1}^{n} E_i \; e^{-\frac{t}{\tau_i}} \; . \tag{5.21}$$

The experimentally determined relaxation modulus (E(t)) master curve (Figure 5.8) was fit to a 14 element Maxwell ladder (Wolcott 1989). The relaxation times (τ_i) were spaced arbitrarily at one per decade of time. A nonlinear regression technique was used to determine the spring moduli (E_i) in Eq. 5.21 from the experimental data. The resulting retardation times (τ_i), and spring moduli (E_i) are repeated here for completeness in Table 5.3.

Table 5.3. Parameters for the Maxwell elements fit to the relaxation modulus master curve. The fitted master curve is shown in Figure 5.10.

Element	E (Pa)	τ (s)
#1	$6.287 \cdot 10^7$	$4.742 \cdot 10^1$
#2	$8.530 \cdot 10^7$	$4.742 \cdot 10^2$
#3	$1.054 \cdot 10^8$	$4.742 \cdot 10^3$
#4	$1.280 \cdot 10^8$	$4.742 \cdot 10^4$
#5	$1.141 \cdot 10^8$	$4.742 \cdot 10^5$
#6	$5.165 \cdot 10^7$	$4.742 \cdot 10^6$
#7	$8.729 \cdot 10^7$	$4.742 \cdot 10^7$
#8	$1.244 \cdot 10^8$	$4.742 \cdot 10^8$
#9	$1.070 \cdot 10^8$	$4.742 \cdot 10^9$
#10	$1.150 \cdot 10^8$	$4.742 \cdot 10^{10}$
#11	$1.052 \cdot 10^8$	$4.742 \cdot 10^{11}$
#12	$1.189 \cdot 10^8$	$4.742 \cdot 10^{12}$
#13	$3.160 \cdot 10^7$	$4.742 \cdot 10^{13}$
#14	$2.028 \cdot 10^8$	$4.742 \cdot 10^{14}$

Figure 5.10 shows the fitted relaxation modulus to the experimentally derived relaxation modulus curve (Figure 5.8) with the 14 element Maxwell model as a function of time.

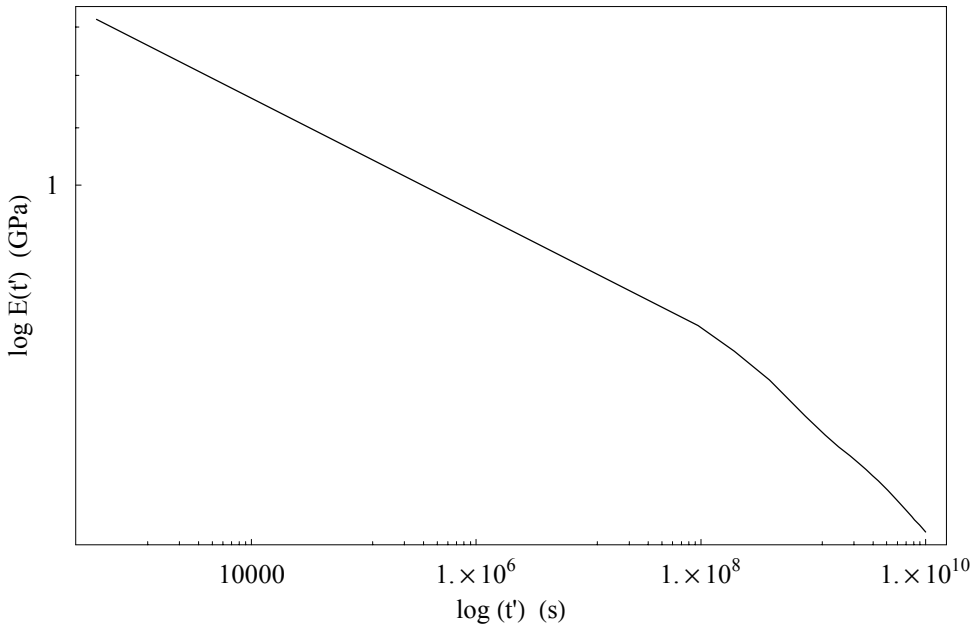

Figure 5.10. The fitted relaxation modulus as function of reduced time (t' = t / a(T,M)). Both axes in logarithmic scale. (Wolcott 1989)

5.3.2.4 Method of Reduced Variables

The relaxation modulus "master curve" describes the long term response of the material at the reference temperature (60 °C) and moisture content (3 %) (Figure 5.8). In order to derive viscoelastic properties at different temperature and moisture levels, the master curve has to be shifted on the time scale with the temperature and moisture shift factor (Figure 5.9). The new time scale is represented by the reduced time (t') which is given by the relation:

$$t' = \frac{t}{a(T, M)}, \tag{5.22}$$

where

t' = reduced time
t = time
$a(T, M)$ = temperature and moisture content shift factor (Eq. 19).

The creep compliance (D(t)) or relaxation modulus (E(t)) of the material can be derived at other than the reference temperature and moisture content conditions by substituting the reduced time in Eq. 5.20 or Eq. 5.21 respectively. Also, to determine the viscoelastic response of a material at environmental conditions different than the reference conditions, t' is substituted for

t in the Boltzmann Integral (Eq. 5.9, 5.10), or in the solution of the differential equation (Eq. 5.17, 5.18). The reduced variable method will be applied to account for the time, temperature, and moisture dependence of the flake properties in the following compression model.

5.3.3 Nonlinear Viscoelastic Behavior of the Mat in Transverse Compression

The loosely formed flake mat is compressed in the transverse direction, while the internal environment is continuously changing during the hot-compression process. The flakes will not be positioned uniformly on the area of the mat. If the randomly formed flake mat is divided into small cross sectional area columns it is apparent that within each column the cumulative thickness of the flakes will be different (Figure 5.11). When an external stress is applied to the mat, the stress will be transferred unevenly among of the flake columns. Consequently, stress is not transferred through the mat uniformly. At thicker areas the stress will be higher.

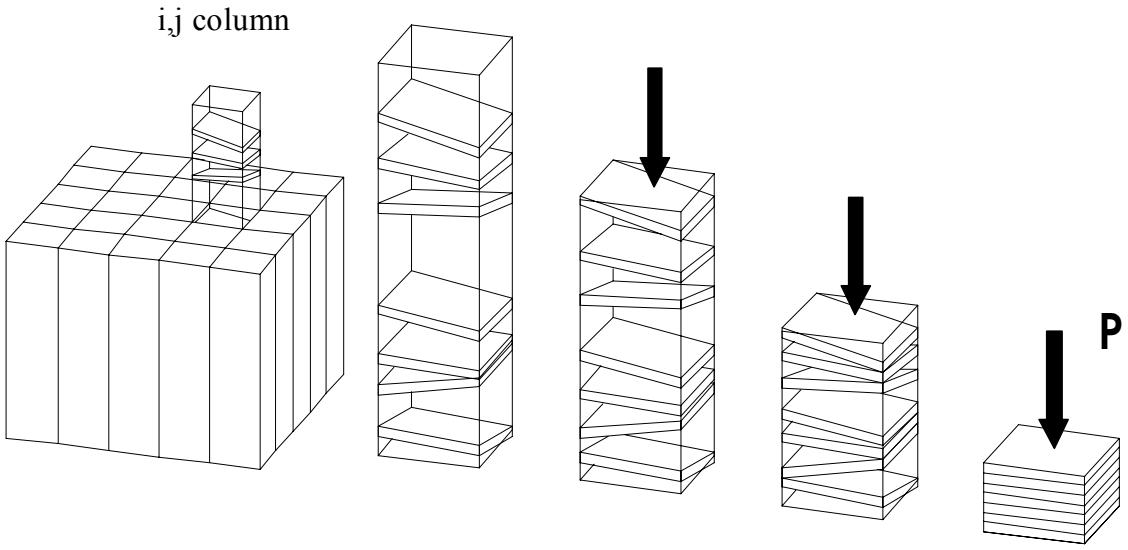

Figure 5.11. Representation of the compression of the strand columns. No stress is required to compress the columns until the flakes form a continuous column (4th column). The stress development in each column is separately controlled by the nonlinear strain function from that position.

Additionally, two levels of cellularity can be identified within the columns. The first level of cellular structure is the consequence of the random flake geometry and deposition process. Space is formed within the mat because of tilting and bridging of the flakes. At the beginning of the pressing process the space is gradually eliminated, however it does not require a substantial pressure (Figure 5.11). As the flakes form continuous flake columns within the mat, further compression starts to collapse the cellular structure of the flakes. This second level of cellular structure has to be consolidated under high pressure to produce good quality boards. As it was mentioned above, the cumulative thickness of the flakes at different horizontal positions in the mat is different. Although the load is applied uniformly over the mat surface, it becomes concentrated in only a small portion of the mat area. Therefore, the consolidation of the continuous flake columns starts at different times during the press schedule. At the beginning of the pressing process the compressed area is small and the localized stresses can be far higher than the applied load. As consolidation progresses, the compressed area rapidly increases and the pressure is continuously redistributed. Consequently, the external load is shared by more and more flake columns within the mat as the density increases. The total stress applied on the flake mat is the summation of the stresses applied for the compression of the individual flake columns.

The compression behavior of the flake columns can be modeled with theories developed to predict the nonlinear response of cellular materials in transverse compression. Additionally, the temperature and moisture are continuously changing within the mat during the press cycle. The high temperature and moisture content plasticizes the flakes. Consequently the compression properties of the flakes are functions of time and space. The time, temperature, and moisture dependence of the properties of the flakes can be described with linear viscoelastic models. Wolcott (1989) proposed that the linear viscoelastic response of the cell wall material to time, temperature, and moisture changes has to be separated from the nonlinear response of the cellular structure. The following two sections summarizes two different approaches for the mathematical representation of the linear viscoelastic and nonlinear transverse compression of the mat.

5.3.3.1 Maxwell Ladder Representation of the Compression Behavior of Flake Columns

The time-dependent response of a viscoelastic material for a complex loading history is provided either by the numerical evaluation of the Boltzmann Convolution Integral or by the governing differential equation of a finite series of Kelvin or Maxwell elements. Several problems arise during the numerical evaluation of the Boltzmann Integral: the solution time is long due to the small time step required for a stable solution, and the full stress or strain history has to be stored to reach a solution. Therefore this solution technique was not considered.

An alternative method is the solution of the governing differential equations of a finite series of Maxwell or Kelvin elements. The following discussion will demonstrate the model development. However, the computation time of this solution also is prohibitive.

During hot-compression the movement of the hot plate is controlled. Therefore, the strain in the mat is known. The unknown is the stress relaxation in each flake column. Consequently several 14 element Maxwell ladders were connected in series to model the time, temperature, and moisture dependent response of individual flake columns. The viscoelastic model is depicted in Figure 5.12.

The governing differential equation of a single Maxwell element is repeated here:

$$\frac{\partial \sigma}{\partial t} = E \frac{\partial \epsilon}{\partial t} - \frac{1}{\tau} \sigma . \tag{5.23}$$

After discretization:

$$\Delta\sigma = E \Delta\epsilon - \frac{1}{\tau} \sigma \Delta t . \tag{5.24}$$

Therefore the iteration formula for a single Maxwell element is

$$\sigma_{i,j,k,n}(t+1) = \sigma_{i,j,k,n}(t) + E_n (\epsilon_{i,j,k}(t+1) - \epsilon_{i,j,k}(t)) - \frac{\Delta t}{\tau_n} \sigma_{i,j,k,n}(t) . \tag{5.25}$$

The temperature and the moisture dependence of the relaxation of the element is taken into consideration by the method of reduced variables. The relaxation time (τ) is reduced with the temperature and moisture shift factor (a(T,M)) as follows:

$$\sigma_{i,j,k,n}(t+1) = \sigma_{i,j,k,n}(t) + E_n (\epsilon_{i,j,k}(t+1) - \epsilon_{i,j,k}(t)) - \frac{\Delta t}{\tau_n \, a(T_{i,j,k},\ M_{i,j,k})} \sigma_{i,j,k,n}(t) . \tag{5.26}$$

The second term in the derived iteration formula is the induced stress due to elastic deformation, and the third term takes into consideration the time, temperature, and moisture dependent stress relaxation. The temperature and moisture content were calculated at the mesh points. The Maxwell ladder representing the material response was positioned between the mesh points, and therefore, the average of the temperatures and moisture contents at the two bounding mesh points were used to calculate the shift factor. The principle of isostrain is valid in each Maxwell element and the resulting stresses are additive in the 14 element Maxwell ladder

$$\sigma_{i,j,k} = \sum_{n=1}^{14} \sigma_{i,j,k,n} . \tag{5.27}$$

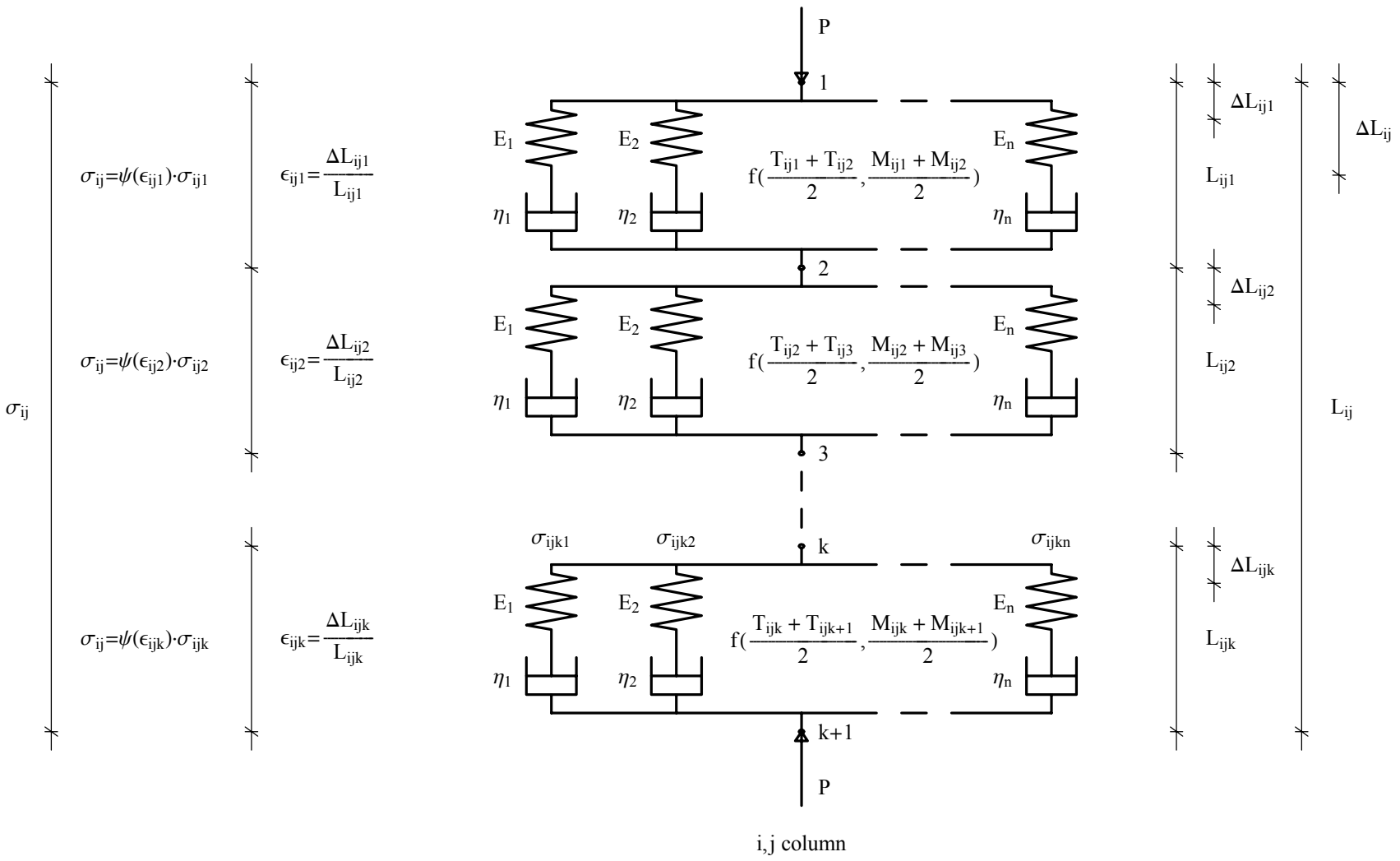

Figure 5.12. Representation of the compression of a flake column by a series of Maxwell ladders.

The principle of isostress would be valid for the Maxwell ladders in series. However, due to the cellular structure of the material, the induced stress in each Maxwell ladder will be different. The nonlinearity of the stress development in the cellular structure of the flake column has to be accounted for by the nonlinear strain function $\psi(\epsilon)$. As it was stated, the nonlinear strain function is a simple multiplier of the linear stresses. It is only a function of the strain in the cellular material and independent of moisture or temperature. However, the relaxation, and therefore, the strain in each Maxwell ladder will be different, which is due to the different temperature and moisture content levels with respect to the vertical position in the flake column. The linear stress, modified with the nonlinear strain function, is equal for each Maxwell ladder, which in turn is equal to the resulting stress on the flake column. The stress induced by the compression on each column is

$$\sigma_{i,j} = \psi(\epsilon_{i,j,1})\,\sigma_{i,j,1} = \psi(\epsilon_{i,j,2})\,\sigma_{i,j,2} = \ldots = \psi(\epsilon_{i,j,k})\,\sigma_{i,j,k}\,. \tag{5.28}$$

A total of k independent equations are written for the Maxwell ladders in series to calculate the strains as follows:

$$\psi(\epsilon_{i,j,k})\,\sigma_{i,j,k} - \sigma_{i,j} = 0\,, \tag{5.29}$$

where $\sigma_{i,j,k}$ is calculated according to Equation 5.27.

The unknowns are the strains at each of the Maxwell ladder ($\epsilon_{i,j,k}$), and the stress in the column ($\sigma_{i,j}$). Therefore, one more equation is needed. It is known that the summation of the displacements in each Maxwell ladder is equal to the displacement of the press plate, consequently:

$$\sum_{i=1}^{k} \Delta L_{i,j,k} = \Delta L_{i,j}\,. \tag{5.30}$$

Knowing the initial length of the Maxwell ladders ($L_{i,j,k}$), the strains in each ladder can be calculated as follows:

$$\epsilon_{i,j,k} = \frac{\Delta L_{i,j,k}}{L_{i,j,k}}\,. \tag{5.31}$$

The solution of the following algebraic equation system will provide the displacements of each Maxwell ladder ($\Delta L_{i,j,k}$), and the stress in each flake column ($\sigma_{i,j}$):

$$\begin{aligned} &\psi(\epsilon_{i,j,1}) \cdot \sigma_{i,j,1} - \sigma_{i,j} = 0 \,, \\ &\psi(\epsilon_{i,j,2}) \cdot \sigma_{i,j,2} - \sigma_{i,j} = 0 \,, \\ &\qquad\qquad \vdots \\ &\psi(\epsilon_{i,j,k}) \cdot \sigma_{i,j,k} - \sigma_{i,j} = 0 \,, \\ &\sum_{i=1}^{k} \Delta L_{i,j,k} = \Delta L_{i,j} \,, \end{aligned} \tag{5.32}$$

where $\sigma_{i,j,k}$ is calculated according to Equations 5.27, and 5.28, and $\epsilon_{i,j,k}$ according to Equation 5.31.

This algebraic equation system has to be solved simultaneously for each of the flake columns under compression at each time step (Δt) to calculate the stress in the column and the displacements in each Maxwell ladder. The resulting algebraic equation system (Eq. 5.32) was solved by HYBRD, a public domain nonlinear equation system solver, developed by Burton (1980). The vertical midplane of the mat was discretized to 361 mesh points, 19 in each direction. Therefore, 19 flake columns were compressed in a row, and 18 Maxwell ladders represented the compression behavior of the flakes between the mesh points within each column. The input parameters of HYBRD were adjusted according to the program description. The error tolerance was set to 10^{-4}, and the stress variable was normalized in order to reach a more stable solution. A solution was calculated within 20 hours on a DEC Alpha workstation with specifics of the computer given in Chapter 3. As the number of the mesh points in the vertical direction was increased, together with the number of equations in the algebraic system, Δt had to be reduced substantially to obtain a stable solution. The computing time increased to a level which was clearly prohibitive to further pursue this solution. Therefore a simplified computational method was developed.

5.3.3.2 Simplified Compression Model

The second method is based on the discretization of the modified Hooke's Law in time. The modified Hooke's Law states that the stress calculated by assuming linear behavior has to be multiplied by the nonlinear strain function to represent the nonlinear response of a cellular material to an induced strain:

$$\sigma = E\,\epsilon\,\psi(\epsilon) \tag{5.33}$$

In this method the stresses in the flake columns are calculated by assuming linear behavior. These stresses are multiplied by $\psi(\epsilon)$ only in the last step of the solution to calculate

the nonlinear response of the material. The flake columns were discretized in the vertical direction as depicted in Figure 5.13.

It was assumed that the relaxation modulus of the material (E(t)) between two mesh points is calculated according to Eq. 5.21. The reduced time principle was used to calculate the time, temperature, and moisture dependence of the relaxation modulus using the fitted shift factor equation (Eq.5.19).

The linear Hooke's Law was considered to describe the linear response of the material between two mesh points. The Hooke's Law was discretized in time using a backward scheme as follows:

$$\frac{\partial \sigma_{i,j}}{\partial t} = \frac{\partial}{\partial t}\left(E_{i,j,k} \cdot \epsilon_{i,j,k}\right) = \frac{\partial E_{i,j,k}}{\partial t}\,\epsilon_{i,j,k} + E_{i,j,k}\,\frac{\partial \epsilon_{i,j,k}}{\partial t} \tag{5.34}$$

$$\Delta\sigma_{i,j}(t) = \Delta \mathrm{E}_{i,j,k} \cdot \epsilon_{i,j,k}(t-1) + E_{i,j,k}(t-1)\,\Delta\epsilon_{i,j,k} \tag{5.35}$$

where

$$\Delta \mathrm{E}_{i,j,k} = E_{i,j,k}(t) - E_{i,j,k}(t-1),$$
$$\Delta\epsilon_{i,j,k} = \epsilon_{i,j,k}(t) - \epsilon_{i,j,k}(t-1).$$

Substituting into Eq. 5.35:

$$\Delta\sigma_{i,j}(t) = \\ \left(E_{i,j,k}(t) - E_{i,j,k}(t-1)\right) \cdot \epsilon_{i,j,k}(t-1) + E_{i,j,k}(t-1) \cdot \left(\epsilon_{i,j,k}(t) - \epsilon_{i,j,k}(t-1)\right). \tag{5.36}$$

Collecting terms:

$$\Delta\sigma_{i,j}(t) = E_{i,j,k}\,(t) \cdot \epsilon_{i,j,k}(t-1) + E_{i,j,k}(t-1) \cdot \epsilon_{i,j,k}(t) - 2 \cdot E_{i,j,k}(t-1) \cdot \epsilon_{i,j,k}(t-1). \tag{5.37}$$

The definition of strain is:

$$\epsilon_{i,j,k}(t) = \frac{\Delta \mathrm{L}_{i,j,k}(t)}{L_{i,j,k}(t-1)}, \tag{5.38}$$

and substituting into Eq. 5.37, and solving for $\Delta \mathrm{L}_{i,j,k}$ gives:

$$\Delta \mathrm{L}_{i,j,k}(t) = \\ \frac{\left(\Delta\sigma_{i,j}(t) - E_{i,j,k}(t) \cdot \epsilon_{i,j,k}(t-1) + 2 \cdot E_{i,j,k}(t-1) \cdot \epsilon_{i,j,k}(t-1)\right) \cdot L_{i,j,k}(t-1)}{E_{i,j,k}(t-1)}. \tag{5.39}$$

This equation provides the displacements between the vertical mesh points within each flake column. All the values at the previous time step (t-1) are known. The relaxation modulus ($E_{i,j,k}(t)$) was calculated from Equation 5.21, and the time, temperature, and moisture dependence of the modulus was accounted for using the reduced time principle.

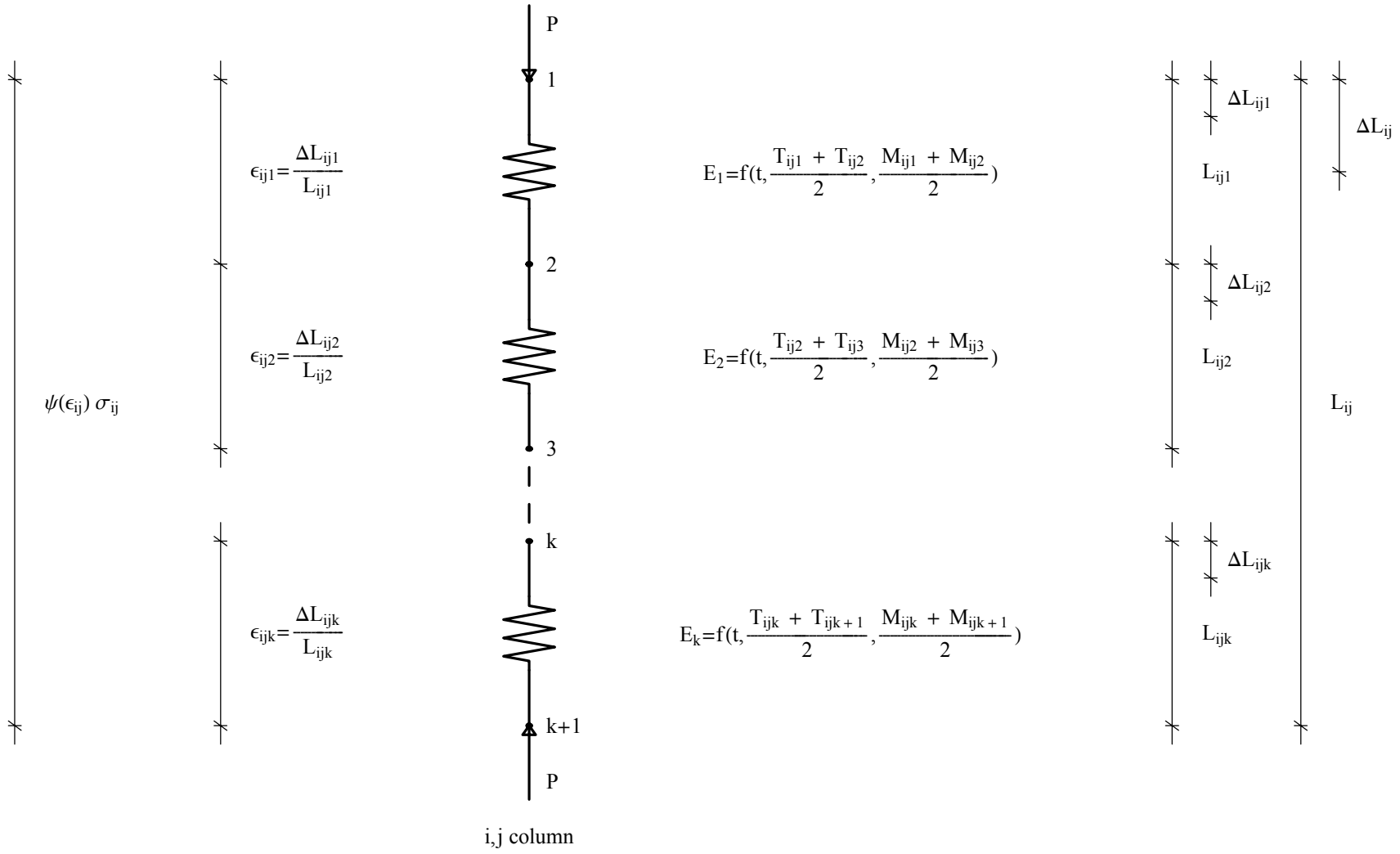

Figure 5.13. Representation of the compression of a flake column by a series of springs. The relaxation modulus of the springs is time temperature and moisture dependent .

The change in the stress on the flake column ($\Delta\sigma_{i,j}(t)$) is determined by recognizing that the sum of the displacements between the mesh points is equal to the displacement of the press platen:

$$\sum_k \Delta \mathrm{L}_{i,j,k}(t) = \sum_k \frac{(\Delta\sigma_{i,j}(t) - E_{i,j,k}(t)\cdot\epsilon_{i,j,k}(t-1) + 2\cdot E_{i,j,k}(t-1)\cdot\epsilon_{i,j,k}(t-1))\cdot L_{i,j,k}(t-1)}{E_{i,j,k}(t-1)} = \Delta \mathrm{L}_{i,j}(t) \tag{5.40}$$

Collecting terms:

$$\Delta \mathrm{L}_{i,j}(t) = \sum_k \frac{L_{i,j,k}(t-1)}{E_{i,j,k}(t-1)}\,\Delta\sigma_{i,j}(t) - \sum_k \left(\frac{E_{i,j,k}(t)}{E_{i,j,k}(t-1)} - 2\right)(\epsilon_{i,j,k}(t-1)\cdot L_{i,j,k}(t-1)), \tag{5.41}$$

and solving for $\Delta\sigma_{i,j}$ gives:

$$\Delta\sigma_{i,j}(t) = \left(\frac{\Delta \mathrm{L}_{i,j}(t) + \sum_k \left(\frac{E_{i,j,k}(t)}{E_{i,j,k}(t-1)} - 2\right)(\epsilon_{i,j,k}(t-1)\cdot L_{i,j,k}(t-1))}{\sum_k \frac{L_{i,j,k}(t-1)}{E_{i,j,k}(t-1)}}\right) \tag{5.42}$$

Eq. 5.42 gives the change in stress in each flake column assuming linear behavior. The change in stress has to be multiplied by the nonlinear strain function $\psi(\epsilon_{i,j})$ to calculate the stress change in the flake column due to the nonlinear response of the cellular structure.

Calculating the change in length according to Eq. 5.39 the final length between two mesh point becomes:

$$L_{i,j,k}(t) = L_{i,j,k}(t-1) - \Delta \mathrm{L}_{i,j,k}(t). \tag{5.43}$$

The volume of the flake column between the mesh points is calculated as follows:

$$V_{i,j,k} = L_x \cdot L_y \cdot L_{i,j,k}(t). \tag{5.44}$$

where

L_x = width of the flake column,
L_y = depth of the flake column.

The mass of the flakes in the flake column was provided by the mat formation model. It was assumed that the mass of the flakes is uniformly distributed between the mesh points. Knowing the mass of the flakes between the mesh points, the density was calculated as follows:

$$\rho_{i,j,k} = \frac{W_{i,j,k}}{V_{i,j,k}}. \tag{5.45}$$

This method did not require the solution of a system of equations, and therefore, a fast solution is achieved. The density distribution of the columns was calculated after each user-defined time step to calculate internal mat conditions. The effect of the change of the internal mat conditions on the relaxation modulus was considered only after each user-defined time step, which further reduced the computational effort. The relaxation modulus ($E_{i,j,k}(t)$) was recalculated as the function of time, temperature, and moisture. Eq. 5.42 and Eq. 5.39 were used to calculate the displacement of the mesh points, and Eq. 5.45 to assess the new vertical density distribution. This solution technique provided a result within 2 hours. The following case study provides the results of a typical simulation run.

5.4 Results of a Simulation Run

The previously described model is able to predict the evolution of the vertical density profile in each imaginary flake column within the structure of the mat. The flake columns are compressed at different times during the press schedule. Due to the varying thickness of the columns, the density profile forms independently in each column. Hence, the density profile of the mat is calculated as the average of the density profiles of the individual flake columns. The model performed well under several simulated compression operations. The basic capabilities of the simulation will be demonstrated under the pressing conditions given in Table 3.1. It has the advantage that the transient temperature and moisture content of the mat during the compression process is readily available, and the influence of temperature and moisture on the density profile formation can be followed. The additional input parameters of the transverse compression model are given in Table 5.4. The density profiles predicted by the model are compared to measured density profiles for various pressing conditions in Chapter 6.

Table 5.4. The compression parameters used in the simulation.

Name	Symbol	Value
Relative density of the flakes*	ρ_r	0.31
Yield strain	ϵ_y	0.015
Expansion Ratio	μ	0.05

* $\rho_r = \frac{\rho_f}{\rho_{cw}}$

Figure 5.14 shows the development of the density profile of the mat as a function of pressing time and vertical position, where the vertical position refers to mesh points. Figure 5.15 shows the average vertical density profile at distinct times during the press cycle as a function of vertical position. It is apparent from Figure 5.14 that the density profile formation occurs during the consolidation, and also after the press has reached final position due to the effect of the migrating heat and moisture on the compressibility of the flakes. Notice, that the density profile has the typical M shape at the end of the compression process, which is generally observed by experiment. This profile is clearly the consequence of the effect of the internal mat conditions on the viscoelastic properties of the flakes. Wang et al. (2000) recommended a methodology to subdivide the density profile formation into two periods and five stages in order to investigate the transient moisture and temperature effects. Figure 5.16 depicts the suggested periods and stages. The consolidation period corresponds to the press closing period, while the adjusting period lasts from the time the press closed to the target thickness till the termination of the press cycle.

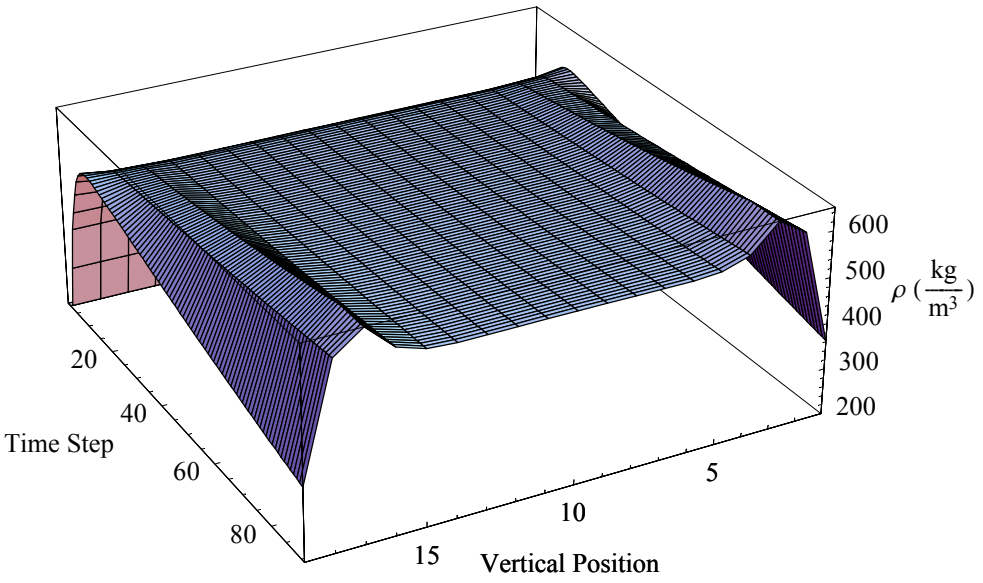

Figure 5.14. The evolution of the average vertical density profile with time. The target mat thickness was 19 mm, and the press time was 480 s.

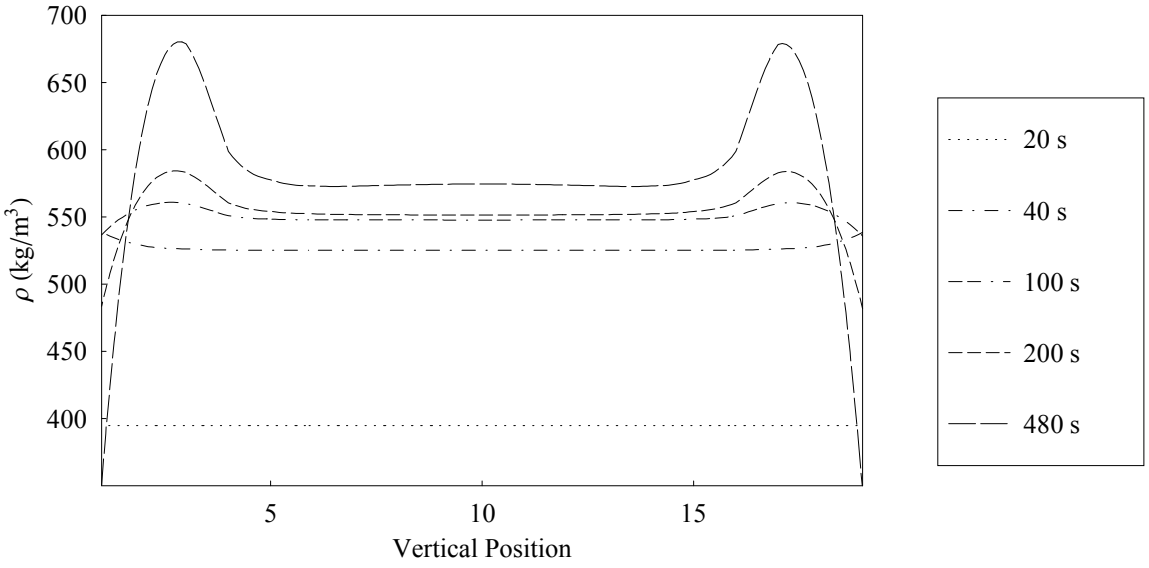

Figure 5.15. The vertical density profile at selected times during the hot-compression. The consolidation (0 to 40 s) and adjusting periods are clearly present on the profile formation.

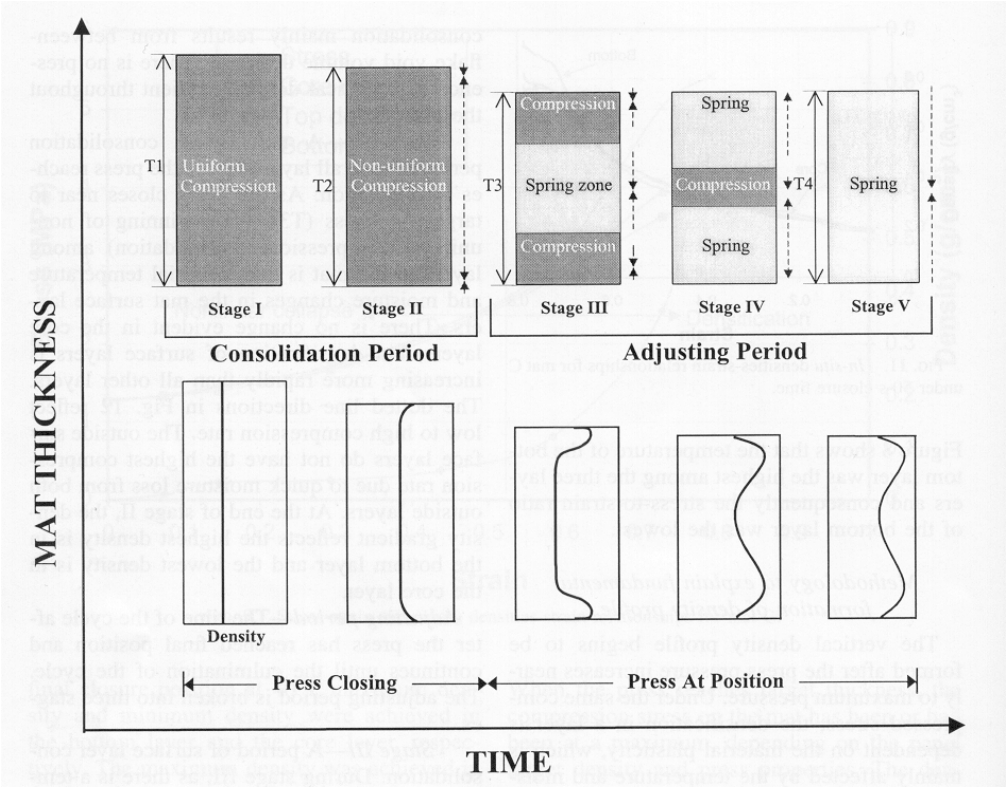

Figure 5.16. The five stages of vertical density profile formation during hot-pressing.(T1 & T2 in-situ thickness of mat being pressed, T3 target thickness of panel, T4 actual thickness of the panel after venting. T1>T2>T3, T4>T3). Stage I: Uniform compression stage. Stage II: Nonuniform compression. Stage III: Surface layer consolidation. Stage IV: Core layer consolidation.. Stage V: Springback. (Wang, S. 2000b)

The first stage of the consolidation period is represented by the uniform increase in density through the thickness of the material. The uniform density increase is the result of the elimination of the voids between the flakes. The migration of heat and moisture within the mat is just initiated, therefore their influence on the density profile formation is negligible. The density profile is flat, as is clearly the case in Figure 5.15 at 20 s in the press cycle.

During the second stage of the consolidation period the quickly rising temperature close to the hot platens plasticizes the material. Flakes closer to the surface are consolidated more than those closer to the center of the mat, resulting in a nonuniform consolidation until the press reaches the target thickness. At the end of the press closing period (40 s), the density profile shows a typical U shape, which is formed by the quickly increasing temperature close to the hot platens (Figure 5.15).

The adjusting period is represented by vigorous temperature and moisture migration in the mat. The formation of the density profile continues during the remainder of the press cycle. During the third stage of the density profile formation, the moisture continuously moves towards

the center of the mat resulting in completely dry face layers. The surface temperature is approaching the platen temperature, forming the largest vertical temperature gradient. The increasing temperature and decreasing moisture at the face layer have opposing effect on the compressibility of the flakes. Therefore the largest consolidation of the mat will not be at the surface, but at some distance from the surface towards the center of the board as is depicted in Figure 5.15 at 100 s in the press cycle.

The fourth stage of the density profile formation can be explained mainly by moisture effects. The temperature gradient will not change substantially in the vertical direction. However, the moisture content of the core layer increases continuously forming the largest vertical moisture gradient in the mat during this period. The moisture will plasticize the flakes at the core, and consequently an increase in core density can be observed in Figure 5.15 at 200 s and 480 s in the press cycle. Also the highest density peak moves slightly towards the center during the press cycle, which is the manifestation of the plasticization effect of the vertically migrating moisture. The predicted density profile at the beginning of the venting period (480 s) shows the typical M shape measured by experiment. Note, that the moisture effect on the compressibility of the flakes is smaller than the temperature effect. Therefore, the density peak is formed closer to the high temperature face of the board than the high moisture content center.

The fifth period is the venting stage in the press schedule, when the press opens up slowly. The mat springs back because the stresses induced by the compression are released. The springback is not uniform throughout the mat thickness. The bond strength of the adhesive has to withstand the sudden increase in thickness, otherwise a panel blow occurs. The prediction of the spring back phenomena requires further improvement of the model.

5.5 Conclusions

A combined nonlinear viscoelastic compression model for the simulation of the consolidation of a wood-based composite mat was presented. The vertical midplane of the mat was subdivided into continuous flake columns of varying thicknesses. The compression of the imaginary columns commence at different times during the press closure, and the vertical density of the mat was considered as the average of the varying density of the flake columns. The time, temperature, and moisture effects on the compressibility of the columns were included in the model through the viscoelastic theory of polymers, and the nonlinear behavior of the mat during consolidation through compression theories developed for man-made cellular materials. The model can predict the development of the vertical density profile among different pressing conditions. A simulation run demonstrated the capability of the model to predict the typical stages of the density profile formation observed during experiments.

Nomenclature

$D(t)$ = Creep Compliance (1 / Pa)
$E(t)$ = Relaxation Modulus (Pa)
E = Young's Modulus (Pa)
E_{cw} = Young's Modulus of the cell wall (Pa)
E_i = modulus of the spring (Pa)
L = dimension of column (m)
M = moisture (%)
T = temperature (K)
T_g = glass transition temperature (°C)

a (T, M) = temperature and moisture shift factor
i = x direction
j = y direction
k = z direction
t' = reduced time (s)
t = time (s)

ϵ = strain
ϵ_y = yield strain of the cell wall (0.015 for wood)
η_i = viscosity of the dashpot (kg / m / s)
μ = expansion ratio
ρ_r = relative density
$\rho_r(\epsilon)$ = relative density function
σ = stress (Pa)
τ = retardation or relaxation time (s)
$\psi(\epsilon)$ = nonlinear strain function

References

Aklonis, J. J., W. J. MacKnight. 1983. Introduction to Polymer Viscoelasticity. John Wiley & Sons, New York, NY.

Back, E. L., L. Salmen. 1982. Glass transition of wood components hold implications for molding and pulping processes. Tappi 65(7):107-110.

Billmeyer, F. W. 1962. Textbook of Polymer Science. John Wiley & Sons, New York, NY.

Dai, C., P. R. Steiner. 1993. Compression behavior of randomly formed wood flake mats. Wood and Fiber Sci. 25(4):349-358.

Dai, C., P. Hubert, S. Chen. 1997. Advances in modeling mat formation and consolidation for wood composite panels. Proceeding of the First European Panel Product Symposium. U.K. 1997. October

Easterling, K. E., R. Harryson, L. J. Gibson, M. F. Ashby 1982. On the mechanics of balsa and other woods. Proc. R. Soc. London A 383:31-41.

Ferry, J. D. 1980. Viscoelastic Properties of Polymers. John Wiley & Sons, New York, NY.

Funakoshi, H., N. Shiriashi, M. Norimoto, T. Akoi. 1979. Studies on the thermoplasticization of wood. Holzforshung 33:159-166.

Gibson, L. J., M. F. Ashby. 1997. Cellular Solids: Structure and Properties. Cambridge University Press, Cambridge, UK.

Harless, T. E. G., F. G. Wagner, P. H. Short, R. D. Seale, P. H. Mitchell, and D. S. Ladd. 1987. A model to predict the density profile of particleboard. Wood and Fiber Sci. 19(1):81-92.

Hubert, P., C. Dai. 1997. Process modeling for wood-based composites. Part 2. A modular approach to modeling mat consolidation during hot-pressing. Proceedings Forest Products Society Structural Panels Technical Interest Group 51st Annual Meeting, Vancouver, British Columbia, Canada

Humphrey, P. E., H. Thoemenn. 2000. The continuous pressing of wood-based panels: an analytical simulation model, its validation and use. Proceedings of the 5th Pacific Rim Bio-Based Composites Symposium, Canberra, Australia, December 10-13. 2000.

Kasal, B. 1989. Behavior of wood under transverse compression. MS. Thesis, V.P.I. & S.U., Blacksburg, VA, USA.

Kelley, S. S., T. G. Rials, W. G. Glasser 1987. Relaxation behavior of the amorphous components of wood. J. of Mat. Sci. 22:617-624.

Kwei, T. K. 1984. The effect of hydrogen bonding on the glass transition temperature of polymer mixtures. J. of Polymer Sci.:Polymer Letters Edition 22:207-313.

Lang, M. E., M. P. Wolcott. 1995. Modeling the consolidation of wood-strand mat. AMD-Vol. 209/MD-Vol. 60, Mechanics of Cellulosic Materials. ASME 1995

Lang, M. E., M. P. Wolcott. 1996. A model for viscoelastic consolidation of wood-strand mats. Part II. Static stress-strain behavior of the mat. Wood and Fiber Sci. 28(3):369-379.

Lenth, C. A. 1994. Investigation of flakeboard mat consolidation. MS. Thesis, V.P.I. & S.U., Blacksburg, VA, USA.

Lenth, C. A., F. A. Kamke. 1996a. Investigations of flakeboard mat consolidation. Part I. Characterizing the cellular structure. Wood and Fiber Sci. 28(2):153-167.

Lenth, C. A., F. A. Kamke. 1996b. Investigations of flakeboard mat consolidation. Part II. Modeling mat consolidation using theories of cellular materials. Wood and Fiber Sci. 28(3):309-319.

Maiti, S. K., L. J. Gibson, M. F. Ashby. 1984. Deformation and energy absorption diagrams for cellular solids. Acta Metall. 32(11):1963-1975.

Maksimov, R. D., V. P. Mocahlov, Y. S. Urzhumstev. 1971. Time-moisture superposition. Mekhanika Polimerov 5780-786.

Maksimov, R. D., E. A. Sokolov, V. P. Mochalov. 1974. Effect of temperature and moisture on the creep of polymeric materials. Part I. One-dimensional extension under stationary temperature-moisture conditions. Mekhanika Polimerov 3:393-399.

Maksimov, R. D., V. P. Mocahlov, E. A. Sokolov. 1975. Influence of temperature and humidity on the creep of polymer materials. Part 3. Shear, and shear and tensile strain acting together. Mekhanika Polimerov 4:627-632.

Maksimov, R. D., V. P. Mochalov, E. A. Sokolov. 1976. Influence of temperature and humidity on the creep of polymer materials. Part IV. Prediction on the basis of field test result. Mekhanika Polimerov 6:982-987.

Meinecke, E. A., R. C. Clark. 1973. Mechanical Properties of Polymeric Foams. Technomic Publishing Co., Westport, USA.

Rosen, S. L. 1993. Fundamental Principles of Polymeric Materials. John Wiley & Sons, New York, NY.

Rush, K. C. 1969. Load compression behavior of flexible foams. Journal of Applied Polymer Science 13:2297-2311.

Salmen, N. L., E. L. Back. 1977. The influence of water on the glass transition temperature of cellulose. Tappi 60(12):137-140.

Salmen, L. 1984. Viscoelastic properties of in-situ lignin under water-saturated conditions. J. Mat. Sci. 19:3090-3096.

Salmen, L., P. Kolseth, A. deRuvo. 1985. Modeling the softening behavior of wood fibers. J. of Pulp and Paper Sci. 11(4):102-107.

Wang, S., P. M. Winistorfer. 2000a. Consolidation of flakeboard mats under theoretical laboratory pressing and simulated industrial pressing. Wood and Fiber Sci. 32(4):527-538.

Wang, S., P. M. Winistorfer. 2000b. Fundamentals of vertical density profile formation in wood composites. Part II. Methodology of vertical density formation under dynamic conditions. Wood and Fiber Sci. 32(2):220-238.

Williams, M. L., R. F. Landel, J. D. Ferry. 1955. The temperature dependence of relaxation mechanisms in amorphous polymers and other glass-forming liquids.

Winistorfer, P. M., W. W. Moschler, S. Wang, E. DePaula. 2000. Fundamentals of vertical density profile formation in wood composites. Part I. In-situ density measurement of the consolidation process. Wood and Fiber Sci. 32(2):209-219.

Wolcott, M. P. 1989. Modeling viscoelastic cellular materials for the pressing of wood composites.. PhD. Dissertation, V.P.I. & S.U., Blacksburg, VA, USA.

Wolcott, M. P., F. A. Kamke, D. A. Dillard. 1990. Fundamentals of flakeboard manufacture: Viscoelastic behavior of the wood component. Wood and Fiber Sci. 22(4):345-361.

Wolcott, M. P., F. A. Kamke, D. A. Dillard. 1994. Fundamental aspects of wood deformation pertaining to manufacture of wood-based composites. Wood and Fiber Sci. 26(4):496-511.